Inadvertent Earth Reentry Breakup Analysis for the New Horizons Mission

Lisa Ling[1], Ahmed Salama[2], Mark Ivanov[2], Angus McRonald[3]

[1]NASA Lyndon B. Johnson Space Center, 2101 NASA Parkway, Houston, TX 77058, USA,
Lisa.M.Ling@nasa.gov
[2]Jet Propulsion Laboratory, 4800 Oak Grove Dr, Pasadena, CA 91109, USA,
ahmed.h.salama@jpl.nasa.gov, mark.c.ivanov@jpl.nasa.gov
[3]Global Aerospace Corporation, 711 W. Woodbury Rd, Suite H, Altadena, CA 91001, USA,
Angus.D.McRonald@gaerospace.com

ABSTRACT

The New Horizons (NH) spacecraft was launched in January 2006 aboard an Atlas V launch vehicle, in a mission to explore Pluto, its moons, and other bodies in the Kuiper Belt. The NH spacecraft is powered by a Radioisotope Thermoelectric Generator (RTG) which encases multiple General Purpose Heat Source (GPHS) modules. Thus, a pre-launch vehicle breakup analysis for an inadvertent atmospheric reentry in the event of a launch failure was required to assess aerospace nuclear safety and for launch contingency planning. This paper addresses potential accidental Earth reentries analyzed at the Jet Propulsion Laboratory (JPL) which may arise during the ascent to parking orbit, resulting in a suborbital reentry, as well as a departure from parking orbit, resulting in an orbital reentry.

1. INTRODUCTION

The New Horizons (NH) spacecraft (see Fig. 1) was launched in January 2006 aboard an Atlas V launch vehicle, in a mission to explore Pluto, its moons, and other bodies in the Kuiper Belt. The NH spacecraft is powered by a Radioisotope Thermoelectric Generator (RTG) which encases multiple General Purpose Heat Source (GPHS) modules. Thus, a pre-launch vehicle breakup analysis for an inadvertent atmospheric reentry in the event of a launch failure was required to assess aerospace nuclear safety and for launch contingency planning. This paper addresses potential accidental Earth reentries analyzed at the Jet Propulsion Laboratory (JPL) which may arise during the ascent to parking orbit, resulting in a suborbital reentry, as well as a departure from parking orbit, resulting in an orbital reentry.
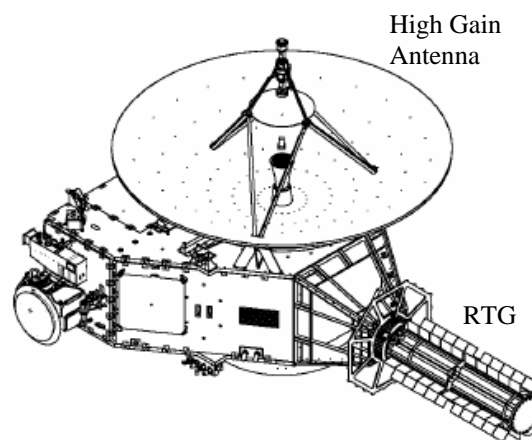

Figure 1. The New Horizons Spacecraft

The suborbital reentries consisted of launch failure scenarios leading to the activation of the Flight Termination System at various times during ascent, resulting in ballistic fallback trajectories. For orbital reentries, the V-Gamma Map consisting of the envelope of possible entry speed (V) and entry flight path angle (gamma) pairs was generated based on the assumption of steady misaligned burns (SMB) while in the parking orbit. Points about the V-Gamma Map as reentry conditions were analyzed, including delayed elliptic where the vehicle reenters the atmosphere after passing through an apogee; prompt elliptic where the vehicle is on a downward path at the end of the burns, approaching a perigee within the atmosphere; powered reentry which occurs while the burns are in progress; and circular orbit decay (COD) due to failed burns in the parking orbit. The potential launch failure scenarios leading to these suborbital and orbital reentries were selected as representative and bounding cases. Additional cases were analyzed to ensure that all potential accident initial conditions (AIC) that were major contributors to accident outcome conditions (AOC) where the RTG experiences a potentially

1

damaging environment were addressed to deliver a complete reentry breakup analysis. The AICs were identified in the accident sequence analysis and progressed logically to various AOCs through Event Sequence Diagrams. These additional major contributor failure scenarios included Liquid Rocket Engine (LRE) catastrophic launch failures and trajectory/attitude control malfunction prior to Earth escape leading to accidental Earth reentry.

The heating rate, integrated heating, and g-loading for the reentry trajectories were computed to assess the potential breakup of the RTG housing and the release of the GPHS modules using integrated heating/g-load failure criteria. The RTG could be shielded from aerodynamic heating during the reentry by the spacecraft bus and High Gain Antenna (HGA). In powered reentry, the Stage III Star 48B motor could also shield the RTG from heating.

Finally, a contingency plan was developed for day-of-launch failure operations in which the expected footprint of the RTG/GPHS modules on the surface of the Earth was determined.

2. V-GAMMA MAP

Based on inputs obtained from [1] including the burn and coast durations and spacecraft masses while in the parking orbit, a V-gamma map for the SMB was developed as shown in Fig. 2 for the purpose of comparing similar SMB categories and exploring the boundary of reentry parameters. The thrust misalignment in the SMB is defined in terms of the cone and clock angles of a sphere. The cone angle is measured in the yaw plane with 0 deg as the nominal burn. The clock angle is about the roll axis with 90 deg for a vertically upward thrust. Fig. 3 shows the relative probabilities for the 5 main categories of outcome: powered entry (PWE), hyperbolic escape (HES), prompt elliptic (ELP), elliptic delayed (ELD), and decay of ellipse (DEL). The vehicle in a PWE enters the atmosphere with the engine/motor still burning. In a HES, the vehicle escapes from the gravitation of the planet at hyperbolic speed. The vehicle in an ELP proceeds with a downward velocity and enters the atmosphere prior to the apogee. In the ELD, the vehicle passes the apogee before entering the atmosphere near the perigee. In addition, there is a category representing a failure to burn, which results in the decay of the parking orbit and ends in a reentry from circular orbit decay (COD). Circular orbit decay is also the end point of the

DEL category. The relative probabilities of the categories presented in Fig. 3 are limited by the assumption of a SMB. The comparison of this mission with the Mars Exploration Rover-A (MER-A) and Pathfinder missions for SMBs is given in Tab. 1.
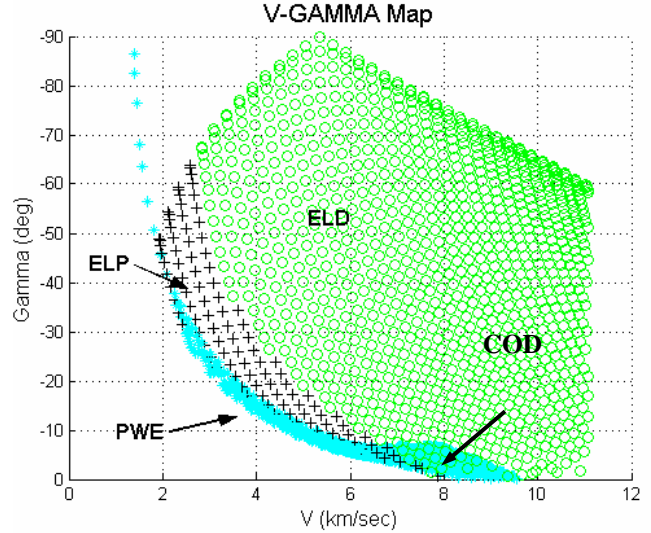

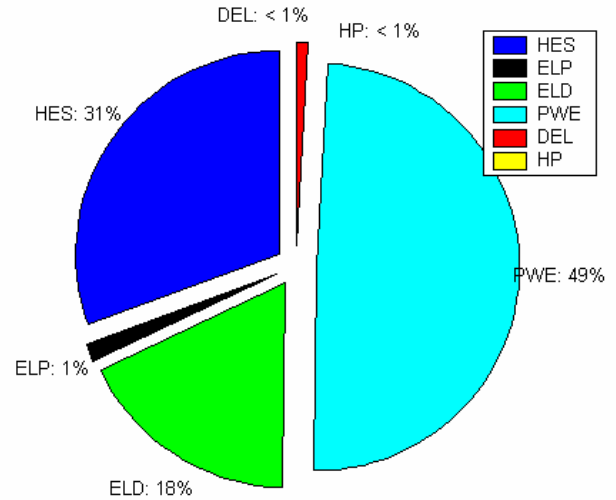*Figure 2. V-Gamma Map for the NH Mission*

Figure 3. Relative Probabilities for the NH mission

Table 1. Percentages for the Steady Misaligned Burn

	Percentages		
Category	**NH**	**MER-A**	**Pathfinder**
Powered Entry	49.0	38.71	38.92
Prompt Elliptic	1.0	5.82	5.76
Delayed Elliptic	18.0	41.11	38.81
Decay of Ellipse	1.0	7.57	5.88
Hyperbolic Escape	31.0	6.79	10.44

It can be seen that the percentage for hyperbolic escape is higher for NH, consistent with the higher launch energy. It is noted that the prompt elliptic cases include some that are hyperbolic, where the vehicle passes through the atmosphere at the end of the burn and possibly performs a multiple-skip entry. Also, the decay of ellipse cases probably reenter as decay of circular orbit, similar to the cases of incomplete burn that leave the vehicle in orbit in vacuum.

For powered reentries, the entry angle-of-attack (AOA) of the vehicle centerline relative to the airflow at 120 km altitude, the reentry altitude, is not random as shown in Fig. 4. The entry time measured from the start of the Centaur second burn is given in Fig. 5. Powered reentry can occur as early as near 134 sec during the Centaur second burn, as well as during the coast and the STAR 48B burn with appropriate mass and thrust accounted for. The non-powered reentries can occur after the STAR 48B burn or after the staging of the STAR 48B motor.
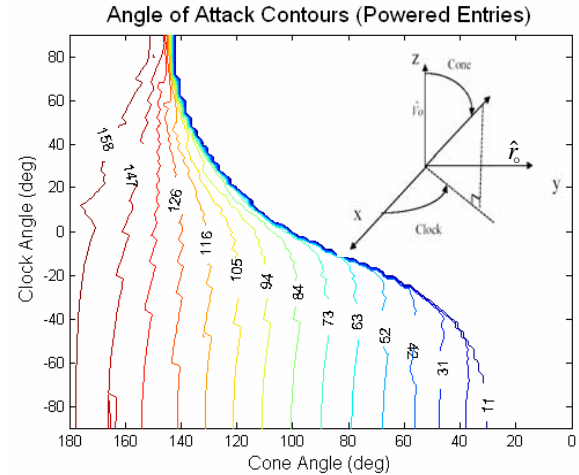

Figure 4. Powered Entry Angle-of-Attack Contours
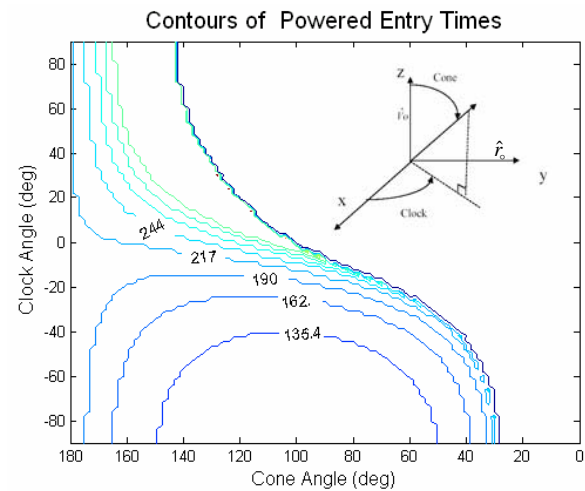
Figure 5. Contours of Powered Entry Times Measured from Start of Second Centaur Burn

3. FAILURE CRITERIA

In prior analyses for the Cassini mission [2], failure criteria for the RTG, i.e., release of the GPHS modules, were defined as a function of the allowable load (g-load) and integrated reference heating (Q_{ref}). The Cassini single lumped-mass model of the RTG was derived from the Galileo multiple node thermal/structural RTG model. The Cassini model as shown in Fig. 6 was used in the NH breakup analysis for RTG failure assessment. For the spacecraft-RTG attachment, the corresponding failure criteria

3

based on a reference 1-ft nose radius cylinder were:

$$Q_{ref} = 15684 \text{ J/cm}^2$$
$$\text{g-load} = 33 \text{ g}$$

This indicates that the RTG case will fail before the attachment. The time integral of the stagnation point heating for HGA failure is 214 J/cm^2.
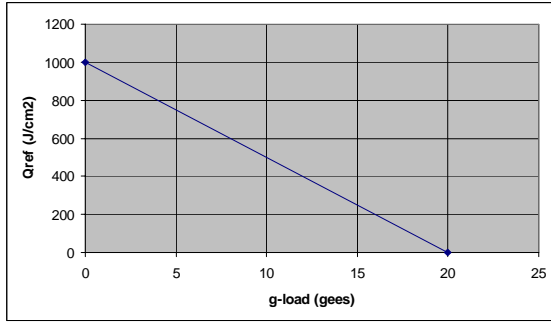

Figure 6. RTG Failure Criteria Based on a Reference 1-ft Nose Radius Cylinder

4. POINTS ABOUT THE V-GAMMA MAP ORBITAL REENTRIES

Entry trajectories have been evaluated for a number of points about the V-gamma map. These points are characterized by the vehicle configuration, thrust misalignment, and associated entry condition that determines the type of reentry. The entry vehicle may be the separated spacecraft or the spacecraft attached to the empty STAR 48B motor. The entry condition at 120 km consists of the angle-of-attack, inertial velocity, and inertial flight path angle (FPA). The powered reentry cases are discussed in detail later in Sec. 4.1.

In the circular orbit decay entry which results from an incomplete burn, including no burn of both of the second Centaur burn and STAR 48B burn, it is assumed that the staging and separation have proceeded as planned, so that the entry vehicle is the spacecraft alone. The entry is random around the Earth, and thus so is the angle-of-attack. In this section, the STAR 48B failure to ignite is not considered. The Atlas second Centaur burn gives the spacecraft the escape velocity it needs to escape the Earth and inserts it into a heliocentric orbit. The STAR 48B burn provides the needed extra speed to get to Pluto.

In this analysis, only the ballistic coefficient of a tumbling spacecraft at Mach 10 has been considered to represent the prompt elliptic, the delayed elliptic, and the circular orbit decay types of reentry. The ballistic coefficient, $m/C_D A$, is 68.7 kg/m^2, where the mass (m) is 465 kg; the drag coefficient (C_D) is 1.82; and the reference area (A) is 3.72 m^2.

The entry conditions for 14 cases of orbital reentry are given in Tab. 2. The table also shows the values of the cone angle A and the clock angle B, relative to the initial direction of the velocity in the intermediate parking orbit, and the angle-of-attack at entry. These 14 points represent the outer boundary of the V-gamma map and are the cardinal points intended to bound the orbital reentry scenarios. The corresponding peak reference stagnation point convective heating, its time integral, and the peak g-load are given in Tab. 3.

Comparing the maximum heating and g-load calculated for each point to the failure criteria shown in Fig. 6, it is concluded that the RTG would fail and release the GPHS modules for points 1, 2, and 5 – 14 since the combined g-load and maximum heating exceeded the allowable limits. The RTG would not break up, however, for points 3 and 4.

Table 2. Entry Conditions of Points About the V-Gamma Map

Point	Cone Angle (deg)	Clock Angle (deg)	Angle of Attack (deg)	Inertial Entry Speed (km/s)	Inertial Entry FPA (deg)
1	124	90	110	4.2	-81.92
2	134	90	86	2.83	-67.62
3	142	90	57	1.93	-48.93
4	140	70	63	2.69	-32.51
5	136	50	63	4.25	-15.15
6	126	30	59	6.58	-5.5
7	90	20	49	10.96	-14.53
8	82	40	62	10.89	-33.48
9	74	70	75	10.96	-54.87
10	80	90	98	10.1	-64.71
11	100	90	127	7.56	-77.69
12	-	-	-	7.77	-0.25
13	146	80	150	2.53	-30.69
14	142	60	115	2.99	-25.44

4

Table 3. Trajectory Parameters for Points About the V-Gamma Map

Point	Type	Max heating rate (W/cm^2)	Integrated Heating* (J/cm^2)	Max g-load (g's)
1	ELD	46.9	507.8	50.2
2	ELD	14.4	220	23.5
3	ELP	4.7	94.6	11.2
4	ELP	8.6	200.2	13.4
5	ELP	22.2	721.6	15.2
6	ELP	54.7	2970	13.7
7	ELD	362.0	6726.6	65.3
8	ELD	537.9	4424.9	155.6
9	ELD	688.9	3774.9	254.9
10	ELD	562.6	3079.7	241.7
11	ELD	255.5	1653.3	159.8
12	COD	42.4	10090	6.7
13	PWE	103.0	1155.6	174.4
14	PWE	150.0	1035.5	72.1

* Based on a reference 1-m nose radius sphere

The maximum heating rate and maximum g-load do not occur at the same time or altitude for any of the trajectories presented above.   The conditions at which the failure criteria are exceeded are shown in Tab. 4.   The times of failure vary significantly for various steep entries and COD.

Table 4. Conditions at Failure of RTG Case in Orbital Reentries

Case	Time From Entry (sec)	Altitude (km)	Integrated Heating* (J/cm^2)	g-load (g)
1	19	40.65	267.7	24.1
2	33	32.96	170.8	19.9
3	-	-	-	-
4	-	-	-	-
5	59	61.89	466.3	10.7
6	72	84.95	756.3	2.1
7	18	87.58	827.7	3.4
8	10	77.96	911.2	16.0
9	7	75.15	790.6	23.
				1
10	7	74.27	668.1	23.0
11	9	60.73	410.1	17.6
12	442	112.03	786.0	0.0
13	52	19.55	1093.6	20.8
14	46	34.62	750.4	7.2

* Based on a reference 1-m nose radius sphere

The g-load was computed based on the normalized non-gravitational perturbing acceleration. The centrifugal and Coriolis accelerations due to the rotation of the Earth were considered in the trajectory propagation, but not in the calculation of the aerodynamic g-load.

The indication from these 14 points in Tab. 4 is that the RTG does not fail in approximately 14.3% of the orbital reentries considered (prompt elliptic, delayed elliptic SMB cases, decay of circular orbit, and powered entries).   In entries where the RTG fails, the GPHS modules are released at altitudes covering a range of 20 – 112 km depending on the large range of entry speeds and flight path angles of the V and gamma entry cases.

For an Earth reentry at about -0.25 deg flight path angle and near the circular orbit speed of 7.8 km/s at 125 km altitude with Earth rotation downwind at latitude 28 deg (408 m/s), the integrated heating is 10,090 J/cm^2 based on a reference 1-m nose radius sphere. The RTG is expected to break up since the integrated heating far exceeds the maximum allowable heating. This circular orbit decay condition represents the most likely launch vehicle failure. For additional reentry configurations consistent with the major failure contributors to the orbital reentry AOC, refer to the Orb1 through Orb4 cases in Sec. 6.

4.1. Powered Reentries

For powered reentries, two cases were simulated where the entry occurs during the STAR 48B burn. The vehicle configuration at entry is the

spacecraft with the STAR 48B motor, spin table, and adapter. The entry mass depends on the fuel remaining at the time of entry, and the vehicle orientation at entry is specified by the entry angle-of-attack. The spacecraft is assumed to tumble following the STAR 48B staging/failure due to aerodynamic instability.

At an entry angle-of-attack of 0º with the spacecraft facing the flow, the STAR 48B motor case will not receive enough heating to play a part in the breakup before the RTG fails. At an entry angle-of-attack of 180º with the nozzle facing the flow, there is essentially no failure until the motor burn ceases, as the exhaust pressure greatly exceeds the stagnation pressure of the flow. Thus, in both scenarios of face-on and end-on entries, the end of burn and separation of the STAR 48B is assumed to occur at the nominal times. In a side-on entry at an entry angle-of-attack of 90º, the STAR 48B failure is assumed to occur at 608 J/cm^2, referenced to a 1-m nose radius sphere, and for an intermediate entry angle-of-attack, the failure integrated heating for the STAR 48B is an inverse function of the sine of the angle-of-attack. The entry vehicle characteristics for the two cases of powered entry are given in Tab. 5.

Table 5. Entry Vehicle in Powered Entries

Case	Mass (kg)	C_D	A_{ref} (m^2)	Ballistic Coefficient (kg/m^2)	STAR 48B Failure Integrated Heating* (J/cm^2)
1	2690	0.18	10.5	1423	1226
2	2287	0.08	10.5	2682	673

* Based on a reference 1-m nose radius sphere

In the first powered reentry case where the entry angle-of-attack is 150º, the vehicle is flying almost end-on. Thus, the spacecraft is shielded from aerodynamic heating by the plume from the burning STAR 48B, and the RTG failure is based on g-load only. In the second powered

entry case where the entry angle-of-attack is 115º, the vehicle is flying approximately side-on and spinning. Thus, the RTG and HGA failures are evaluated based on combined g-load and integrated heating. In both powered reentry cases, the RTG fails, and the GPHS modules are released (see powered entry cases 13 and 14 in Tab. 2 and 3 for trajectory parameters and in Tab. 4 for conditions at failure of RTG case).

5. SUBORBITAL BALLISTIC FALLBACK TRAJECTORIES

In this section a number of ballistic fallback trajectories from a nominal ascent trajectory ([3] and [4]) prior to reaching the parking orbit is investigated. Tab. 6 gives the time, altitude, velocity, and flight path angle at the cessation of thrust during ascent. The peak stagnation point reference heating, its time integral, and the peak g-load in Tab. 7 are quantified to determine if it is likely that the RTG breaks up or separates from the spacecraft prior to surface impact. This is not a complete breakup analysis, but rather a quick analysis based on the heating time integral and maximum g-load.

In this failure scenario, the activation of the Flight Termination System (FTS) including the Breakup System (BUS) following thrust cessation is assumed, resulting in a tumbling spacecraft as the reentry vehicle. Note that this configuration became inapplicable after a contingency procedure was added to disable the BUS at 40 sec MET, resulting in a tumbling S/C + an almost intact STAR 48B with nearly all of the solid propellant as the reentry vehicle. However, the result of the suborbital reentry cases that are no longer relevant is not updated since the prediction of the RTG failure is assumed not to change significantly by changing the reentry configuration. This assumption is made considering that the addition of the almost intact STAR 48B to the tumbling entry vehicle does not significantly change the exposure of the RTG case to the flow. For additional reentry configurations consistent with the major failure contributors to the suborbital reentry AOC, refer to the Sub1 through Sub3 cases in Sec. 6.

Table 6. Initial Conditions of Ballistic Fallback Trajectories

Case	Time of Thrust Cessation	Altitude (km)	Inertial Velocity (m/s)	Inertial FPA (deg)

	From Launch (sec)			
1	100.00	41.01	1333	34.88
2	150.00	78.38	2082	19.95
3	200.00	111.77	3176	11.16
4	250.00	140.18	5048	6.22
5	300.00	165.29	5963	4.18
6	350.00	183.71	6133	2.85
7	400.00	196.08	6322	1.75
8	450.00	203.34	6530	0.89
9	500.00	206.52	6754	0.26
10	520.00	206.90	6849	0.07
11	540.00	206.87	6946	-0.08
12	560.00	206.53	7046	-0.20
13	580.00	205.94	7148	-0.27
14	600.00	205.19	7253	-0.32

Table 7. Trajectory Parameters for Ballistic Fallback Trajectories

Case	Max Heating Rate (W/cm²)	Integrated Heating* (J/cm²)	Max g-load (g's)
1	2.2	46.3	4.5
2	3.9	186.9	6.4
3	12.1	516.7	10.4
4	36.8	1559	14.1
5	53.4	2741.5	14.4
6	56.6	3040.1	14.2
7	59.3	3405.8	13.5
8	61.5	3879.6	12.6
9	62.2	4529.3	11.3
10	61.8	4869.1	10.7
11	60.8	5292.1	10.0
12	58.9	5825.0	9.1
13	55.7	6604.9	8.1
14	49.4	8007.4	7.1

* Based on a reference 1-m nose radius sphere

Referring to the failure criteria shown in Fig. 6 and explained in Sec. 3, it appears that the RTG would likely survive in cases 1 and 2. In cases 3 through 14, the failure criteria are exceeded, and the corresponding conditions are given in Tab. 8.

When thrust is terminated up to a time between 150 and 200 sec, the RTG survives and impacts the ocean. When it is terminated between that time to a time between 540 and 560 sec MET, the released GPHS modules would impact the ocean. Released GPHS modules would impact Africa when the thrust is terminated between that

time and a time between 600 and 620 sec MET. For failures after that time, the spacecraft will be captured into orbit.

Table 8. Conditions at Failure of RTG Case in Fallback Trajectories

Case	Time** (sec)	Altitude (km)	Integrated Heating* (J/cm²)	g-load (gees)
1	-	-	-	-
2	-	-	-	-
3	101	36.46	457.7	10.4
4	71	58.25	663.2	4.32
5	69	65.40	762.3	2.59
6	69	67.90	739.8	2.03
7	72	69.38	598.0	1.79
8	76	72.03	770.8	1.31
9	84	74.87	792.7	0.91
10	88	76.80	593.4	0.70
11	95	78.32	784.9	0.57
12	105	80.36	794.7	0.43
13	121	83.39	785.7	0.26
14	158	88.36	779.0	0.11

* Based on a reference 1-m nose radius sphere
** Time from failure or time from entry if spacecraft temporarily exits atmosphere

6. REENTRIES FOR THE MAJOR CONTRIBUTORS TO THE AOCs

Although the suborbital and out-of-orbit reentries mentioned above are representative and bounding cases, they do not necessarily correspond to the major initiating failure contributors to suborbital and orbital AOCs. Therefore, potential failure scenarios that are major contributors to suborbital/orbital reentry AOCs which were not already included in the previous suborbital and orbital reentry cases were also examined.

The following scenarios/launch vehicle configurations were investigated, where Sub# is a suborbital reentry and Orb# is an orbital reentry:

Sub1: Trajectory control malfunction occurs during ascent between 108.2 and 207.5 or 286.6 and 622.1 sec. The FTS was not activated, either due to its failure or the malfunction was undetected. The outcome is a suborbital reentry before the Centaur second burn in an off-

nominal trajectory, occurring after 622 sec where CDS is disabled, thus resulting in no FTS. Reentry and ground impact occur before the Centaur second burn would have occurred. The reentry configuration is the spacecraft + STAR 48B with all of the solid propellant + Centaur with liquid propellant for the second burn, flying face-on with spacecraft leading.

Sub2: Attitude control malfunction or Centaur LRE catastrophic failure occurs during ascent between 286.6 and 622.1 sec. The CDS is activated late, but before 611 sec during the Centaur first burn. The reentry configuration is the spacecraft + an almost intact STAR 48B with nearly all of the solid propellant, tumbling and no thrust.

Sub3: Attitude control malfunction or Main Engine LRE catastrophic failure during ascent. The CADS is activated during Main Engine burn before 268.6 sec. The reentry configuration is the spacecraft + an almost intact STAR 48B with nearly all of the solid propellant, tumbling and no thrust.

Orb1: Attitude control malfunction occurs during the Centaur second burn between 1732.6 and 2651.7 sec (Centaur second burn through space vehicle separation while in the parking orbit). There is no FTS activation. Halfway into the Centaur second burn, the attitude control malfunction is assumed to lead to tumbling in the vehicle. The onboard sensors detect tumble, triggering Centaur engine cut-off and blow-down, and no spin-up or ignition of the STAR 48B. The partial Centaur second burn with arbitrary attitude brings the vehicle into an orbital reentry. The reentry configuration is the spacecraft + empty Centaur + STAR 48B with all of the solid propellant, tumbling and no thrust.

Orb2: Centaur LRE catastrophic failure, e.g. an explosion, occurs while in the parking orbit. There is no FTS activation. The explosion is assumed to be isolated to the Centaur, which occurs halfway into the Centaur second burn, and the vehicle begins to tumble. Therefore, there is no STAR 48B spin-up, burn, or staging. The partial Centaur second burn takes the vehicle out of the parking orbit, and reentry

occurs due to the decay of this elliptical orbit. The reentry configuration is the spacecraft + STAR 48B with all of the solid propellant, tumbling and no thrust.

Orb3: Attitude control malfunction or Centaur LRE catastrophic failure during ascent between 286.6 and 622.1 sec. The CDS is activated between 611 and 622 sec during the Centaur first burn. The launch vehicle has enough energy to capture into orbit. Reentry occurs from circular orbit decay. The reentry configuration is the spacecraft + an almost intact STAR 48B with nearly all of the solid propellant, tumbling and no thrust.

Orb4: Centaur misaligned burn occurs while in the parking orbit between 1732.6 and 2306.7 sec. Assume the same misalignment in the STAR 48B burn. Powered orbital reentry occurs, and the reentry configuration is the spacecraft + STAR 48B burning.

The outcomes of the above cases are given in Tab. 9. Note that in the Sub3 failure scenario, the suborbital reentry will lead to impact in the ocean and is thus not simulated to expedite the analysis. For the Orb4 failure scenario, refer to the two powered reentry cases presented in Sec. 4.1 for the outcome of the RTG. In all the major contributor cases analyzed, the RTG fails, and the GPHS modules are released.

Table 9. Conditions at Failure of RTG Case in Major Contributor Failure Scenarios

Case	Time from Entry (sec)	Altitude (km)	Integrated Heating* (J/cm^2)	g-load (gees)
Sub1	146	108.1	196	0.0
Sub2	145	90.6	619	0.02
Sub3	N/A**	N/A**	N/A**	N/A**
Orb1	50	84.2	626	0.22
Orb2	298	101.97	618	0.0
Orb3	304	102.69	616	0.0
Or	N/A	N/A*	N/A**	N/A

Ca se	Tim e from Entr y (sec)	Altit ude (km)	Integr ated Heatin g* (J/cm^2)	g- load (gees)
b4	***	**	*	***

* Based on a reference 1-m nose radius sphere
** Ocean impact, not analyzed
*** See Sec 4.1 for 2 powered entry cases

7. CONTINGENCY PLAN FOR DAY OF LAUNCH

The analysis described in the previous sections was used to ultimately assess the probability of accidental Earth reentry and the outcome of the RTG in support of the required nuclear safety assessment process. This section will address the process that was developed to support on day of launch in the event that an in-flight failure actually occurred. The main objective of this process was to determine the approximate most likely impact location of the RTG on the Earth's surface, along with an associated uncertainty impact ellipse, within 30 minutes from receipt of the reentry state vector.

It was assumed that the following Earth reentry state parameters would be available from range safety assets supporting day of launch operations: altitude, latitude, longitude, speed, flight path angle, and flight azimuth. Entry ballistic coefficient of the vehicle was also needed to form a complete state vector set; however, this data was not expected to be available in the supplied state parameters. Therefore a finite list of vehicle configurations and attitude conditions was generated to estimate the most likely ballistic coefficients resulting from the possible in-flight failure scenarios. These configurations are presented in Tab. 10. The selection of the most likely ballistic coefficient would be made in real time based on the timing from launch when the failure scenario occurred.

Table 10. Ballistic Coefficients for Various Configurations

Configuration*	Scenario	Ballistic Coefficient (kg/m^2)
Partial Star48 + s/c (tumbling)	Command destruct during ascent phase	299

Centaur + Star48 + s/c (tumbling)	Failure in Parking Orbit	766
Star48 + s/c (tumbling)	Failure in Parking Orbit	373
s/c Only (tumbling)	Failure in Parking Orbit	72

* Powered reentry was not considered due to the extremely low probability of occurrence.

A trajectory simulation would then be performed starting from the supplied state vector data, including the derived ballistic coefficient, to generate a nominal impact location. In addition, dispersed trajectory simulations would be run to generate an uncertainty impact ellipse. The error sources modeled in these dispersed simulations, along with their values, are presented in Tab. 11.

Table 11. Impact Uncertainty Ellipse Error Sources

Error Source	Value
Inertial Flight Path Angle	+/- 0.1 degree
Speed	+/- 0.1 %
Lift/Drag	+/- 0.03
Mass	+/- 1.0 %
Drag Coefficient	+/- 10 %
Aerodynamic Reference Area	+/- 10 %
Side Force	45 degree bank angle

As added fidelity to the trajectory simulations, winds were accounted for by utilizing actual day of launch measured horizontal wind speeds and directions from the closest NOAA weather station to the nominal impact location. This process involved taking the no wind nominal impact location and feeding it into a software program that automatically determined from the NOAA website the nearest NOAA weather station, checked the availability of wind data from that station (and if no wind were available, checked the next closest station and so on until wind data was available), and downloaded the

wind data into a wind file as input to the trajectory simulation tool.

The process was also designed to be resilient to computer failures that may have prevented detailed trajectory simulations from being performed in real time. This required the pre-generation of a trajectory database that was loaded onto several desktop computers that were available in real time if the JPL main frame computer went down for any reason. This database was generated by varying entry speed, flight path angle, and ballistic coefficient in an attempt to envelop all possible reentry scenarios. For each trajectory data point, a range angle was determined from entry to GPHS impact. Assuming that this range angle is somewhat insensitive to entry location and flight azimuth, an approximate impact location can be determined by rotating the entry position vector in the plane of the flight azimuth by the range angle as determined by a triple table lookup in entry speed, flight path angle, and ballistic coefficient. A representative uncertainty ellipse would then be applied (i.e. the database did not account for uncertainties in simulation parameters).

The entire launch contingency process as described above was tested through several launch rehearsals and was on ready status during the New Horizons launch operations. Fortunately, the launch was near perfect and the process was not exercised in real time.

8. SUMMARY

A pre-launch vehicle breakup analysis of potential inadvertent Earth reentry scenarios in the event of a launch failure was performed for the purpose of assessing aerospace nuclear safety and for launch contingency planning. In the case of an orbital reentry from circular orbit decay, which is the most likely scenario for the orbital reentry AOC, the GPHS modules will be released during the entry. In the majority of the orbital reentry cases of a steady misaligned burn, the GPHS modules will be released prior to surface impact. After considering g-loading and heating, the RTG will reach the surface intact in only about 14.3% of the steady misaligned burn cases. The RTG breakup altitudes ranged from 20 to 112 km.

In the analysis of ballistic fallback trajectories in suborbital reentries, the RTG will survive g-loading and heating to fall back into the ocean for Centaur first burn thrust termination failures

prior to a time between 150 and 200 sec MET. For thrust failures between that time and a time between 540 and 560 sec MET, the RTG is expected to break up and the released GPHS modules to fall back into the ocean. Released GPHS modules would impact Africa when the thrust is terminated between that time and a time between 600 and 620 sec MET. For launch vehicle failures occurring after that time, the vehicle consisting of the spacecraft, STAR 48B, and Centaur will continue into orbit.

The failure scenarios consistent with the major contributors to the suborbital and orbital reentry AOCs were analyzed. In all of these simulated suborbital (Sub1, Sub2, and Sub3) and orbital (Orb1, Orb2, Orb3, and Orb4) reentries, the RTG failed and the GPHS modules were released. The RTG breakup altitudes ranged from 84 to 108 km.

For day of launch support, a process was developed to provide rapid response in the event that an in-flight failure actually occurred. Through this process, the approximate most likely impact location of the RTG on the Earth's surface would be determined, along with an associated uncertainty impact ellipse.

9. REFERENCES

1. Stabb J., *mass_angus2_update.ppt*, File provided to Angus McRonald on Feb 27, 2004
2. A. McRonald, *Release of RTG Modules from the Cassini Spacecraft during Inadvertent Earth Reentry: General V-Gamma Case*, JPL IOM 312/94.6-783, to L Reinhart, Sep 30, 1994
3. Stabb J., *Fframe.6matrix.saroutp*, File provided to Ahmed Salama on Feb 11, 2004
4. *Non-Launch Services Task Order NLSL-010 Launch Vehicle Nuclear Safety Databook Support for Atlas V*, Pluto – New Horizons, Task D: Chapter 7, Preliminary Representative Mission Trajectory and Timeline Data, Jan 21, 2004